



Diagnostic for Verifying the Thrust Vector Requirement of the AEPS Hall-Effect Thruster and Comparison to the NEXT-C Thrust Vector Diagnostic

*Gabriel F. Benavides, Jonathan A. Mackey, Drew M. Ahern, and Robert E. Thomas
Glenn Research Center, Cleveland, Ohio*

NASA STI Program . . . in Profile

Since its founding, NASA has been dedicated to the advancement of aeronautics and space science. The NASA Scientific and Technical Information (STI) Program plays a key part in helping NASA maintain this important role.

The NASA STI Program operates under the auspices of the Agency Chief Information Officer. It collects, organizes, provides for archiving, and disseminates NASA's STI. The NASA STI Program provides access to the NASA Technical Report Server—Registered (NTRS Reg) and NASA Technical Report Server—Public (NTRS) thus providing one of the largest collections of aeronautical and space science STI in the world. Results are published in both non-NASA channels and by NASA in the NASA STI Report Series, which includes the following report types:

- **TECHNICAL PUBLICATION.** Reports of completed research or a major significant phase of research that present the results of NASA programs and include extensive data or theoretical analysis. Includes compilations of significant scientific and technical data and information deemed to be of continuing reference value. NASA counter-part of peer-reviewed formal professional papers, but has less stringent limitations on manuscript length and extent of graphic presentations.
- **TECHNICAL MEMORANDUM.** Scientific and technical findings that are preliminary or of specialized interest, e.g., “quick-release” reports, working papers, and bibliographies that contain minimal annotation. Does not contain extensive analysis.
- **CONTRACTOR REPORT.** Scientific and technical findings by NASA-sponsored contractors and grantees.
- **CONFERENCE PUBLICATION.** Collected papers from scientific and technical conferences, symposia, seminars, or other meetings sponsored or co-sponsored by NASA.
- **SPECIAL PUBLICATION.** Scientific, technical, or historical information from NASA programs, projects, and missions, often concerned with subjects having substantial public interest.
- **TECHNICAL TRANSLATION.** English-language translations of foreign scientific and technical material pertinent to NASA's mission.

For more information about the NASA STI program, see the following:

- Access the NASA STI program home page at <http://www.sti.nasa.gov>
- E-mail your question to help@sti.nasa.gov
- Fax your question to the NASA STI Information Desk at 757-864-6500
- Telephone the NASA STI Information Desk at 757-864-9658
- Write to:
NASA STI Program
Mail Stop 148
NASA Langley Research Center
Hampton, VA 23681-2199



Diagnostic for Verifying the Thrust Vector Requirement of the AEPS Hall-Effect Thruster and Comparison to the NEXT-C Thrust Vector Diagnostic

*Gabriel F. Benavides, Jonathan A. Mackey, Drew M. Ahern, and Robert E. Thomas
Glenn Research Center, Cleveland, Ohio*

Prepared for the
Propulsion and Energy Forum and Exposition
sponsored by the American Institute of Aeronautics and Astronautics
Cincinnati, Ohio, July 9–11, 2018

National Aeronautics and
Space Administration

Glenn Research Center
Cleveland, Ohio 44135

Acknowledgments

The authors would like to thank the Space Technology Mission Directorate through the Solar Electric Propulsion Technology Demonstration Mission Project for funding the development of this diagnostic as well as for providing funding for the development of the HERMeS Hall thrusters. Additionally, the authors would like to thank Jim Myers and Dale Robinson of Vantage Partners, LLC for their assistance performing thermal modeling for the TVR design. The authors would also like to thank Thomas Haag, Daniel Herman, Wensheng Huang, Dave Jacobson, Hani Kamhawi, Peter Peterson, George Soulas, Robert Thomas, and John Yim for their technical support and guidance on this work. Finally, the authors would like to thank Kevin Blake, Matt Daugherty, Josh Gibson, Roland Gregg, Evelyn Hill, George Jacynycz, Chad Joppeck, Jim Szelagowski, Taylor Varouh, Dave Yendriga, Jim Zakany, and all of the engineers and technicians of the Space Environment Test Branch for assisting with the setup of the TVD, for fabrication of various components, and for operation of the vacuum facilities.

This report contains preliminary findings,
subject to revision as analysis proceeds.

Trade names and trademarks are used in this report for identification
only. Their usage does not constitute an official endorsement,
either expressed or implied, by the National Aeronautics and
Space Administration.

Level of Review: This material has been technically reviewed by technical management.

Available from

NASA STI Program
Mail Stop 148
NASA Langley Research Center
Hampton, VA 23681-2199

National Technical Information Service
5285 Port Royal Road
Springfield, VA 22161
703-605-6000

This report is available in electronic form at <http://www.sti.nasa.gov/> and <http://ntrs.nasa.gov/>

Diagnostic for Verifying the Thrust Vector Requirement of the AEPS Hall-Effect Thruster and Comparison to the NEXT-C Thrust Vector Diagnostic

Gabriel F. Benavides, Jonathan A. Mackey, Drew M. Ahern, and Robert E. Thomas
National Aeronautics and Space Administration
Glenn Research Center
Cleveland, Ohio 44135

Abstract

A diagnostic has been designed and fabricated to verify the thrust vector requirement for the Advanced Electric Propulsion System (AEPS) Hall-effect thruster. This diagnostic will be used to verify that the propulsion system thrust vector offset from the mounting surface normal vector does not exceed 1.5° over the entire throttling range and over the course of 23,000 h of thruster testing. The diagnostic will not violate the thruster's required voltage standoff capability in the presence of carbon backsputter by being minimally intrusive and not significantly adding to the facility backspattered rate. Based on AEPS requirements and numerous facility considerations, an appropriate thrust vector diagnostic design was determined and comprises of a linear array of 23 Faraday probes swept through the plume in a semicircular arc 1 m from the thruster center, which maps the beam current density. The beam current density centroid of the plume is assumed to track the thrust vector within an acceptable level of uncertainty. Additionally, a reference system, including optical alignment to the mounting surface normal vector and tilt sensors, was devised to periodically calibrate the probe position and motion throughout the long duration wear test campaign. Initial measurements of the thruster plume have been acquired to demonstrate the diagnostic's functionality, verify procedures, and assess any necessary improvements prior to implementation of the diagnostic during the AEPS Engineering Development Unit (EDU) long duration wear test. To illustrate the merits of differing approaches to thrust vector determination for different classes of electric propulsion thrusters, NASA's Evolutionary Xenon Thruster-Commercial (NEXT-C) thrust vector diagnostic design details and recent data are also discussed (Appendix A).

Introduction

For missions beyond low Earth orbit, spacecraft size and mass can be dominated by onboard chemical propulsion systems and propellants that may constitute more than 50 percent of spacecraft mass. This impact can be substantially reduced through the utilization of Solar Electric Propulsion (SEP) due to its significantly higher specific impulse. Studies performed for NASA's Human Exploration and Operations Mission Directorate (HEOMD) and Science Mission Directorate (SMD) have demonstrated that a 40 kW-class SEP capability can be enabling for both near-term and future spacecraft architectures (Ref. 1). Since 2012, NASA has been developing a 13 kW Hall-effect thruster electric propulsion string that can serve as the building block for a 40 kW-class SEP capability (Ref. 2).

The 13 kW Hall thruster system development, led by the NASA Glenn Research Center and the Jet Propulsion Laboratory, began with maturation of the high-power Hall Effect Rocket with Magnetic Shielding (HERMeS) thruster and power processing unit. The technology development work transitioned to Aerojet Rocketdyne following a competitive procurement selection for the Advanced Electric Propulsion System (AEPS) contract. The AEPS contract includes the development, qualification, and multiple flight 13 kW electric propulsion string deliveries. The AEPS Electric Propulsion (EP) string consists of the Hall thruster, power processing unit (including digital control and interface functionality),

xenon flow controller, and associated intra-string harnesses. NASA continues to support the AEPS development leveraging in-house expertise, plasma modeling capability, and world-class test facilities. NASA also executes AEPS and mission risk reduction activities to support the AEPS development and mission application.

This paper reviews the progress of one such risk reduction activity, the development of a diagnostic to reliably infer the direction of the 13 kW Hall thruster's thrust vector throughout long duration testing. The speed, magnitude, and predictability of the deviations of the thrust vector from the mounting surface normal vector will have important future implications regarding the necessary capabilities of spacecraft gimbals, avionics, and flight software.

This paper specifically describes the design and development of the AEPS Thrust Vector Diagnostic (TVD), including (i) definition of diagnostic objectives, (ii) literature review of existing EP thrust vector diagnostics, (iii) analyses performed to guide development of the AEPS TVD, (iv) discussion of the selected AEPS TVD design, and (v) initial plume measurements recently acquired with the AEPS TVD to demonstrate functionality, verify procedures, and assess any necessary improvements prior to implementation of the diagnostic during the AEPS Engineering Development Unit (EDU) long duration test. The AEPS diagnostic consists of three interdependent systems, the probe, the reference, and the electronics package.

The probe is colloquially referred to as the Thrust Vector Probe (TVP). While the author shall maintain the convention of referring to the probe as a TVP, most TVPs could be more accurately referred to as *Beam Current Centroid Probes*. The AEPS TVP, like most other thrust vector probes, does not measure the thrust vector directly, but infers the thrust vector based on the assumption of a strong correlation to the behavior of the beam current density centroid. Based on various plume measurements, this is likely a reasonable assumption within a small degree of uncertainty. For the purposes of verifying that the AEPS thrust vector requirement is met, the authors will apply the described assumption and carry an associated uncertainty in the data analysis.

The AEPS TVP is a linear array of Faraday probes that is swept in a 1-m semicircular arc through the thruster's plume. Because the TVP is not static, accurately tracking the absolute location and orientation of the probe relative to the thruster mounting surface normal vector is critical to properly interpreting data collected with the TVP. Without a reference system, the measurements made by the TVP would only provide relative changes in the thrust vector over short durations without the ability to correct for shifts in the vacuum facility structure, thermally induced movement of the thrust stand platform, movement of the thruster's mounting surface, loss of calibration of the motion stages locating the probe's position, or shifts in the relative location of the motion stages to the thrust stand as one might anticipate over a 23,000-h test. Development of the Thrust Vector Reference (TVR) system has been as significant of an undertaking as development of the TVP and shall be discussed later in detail.

The final aspect of the thrust vector diagnostic is the Thrust Vector Electronics (TVE) package. The electronics consist of an array of shunts, protection circuitry, power supplies, data acquisition equipment, and software. The electronics perform the essential function of accurately measuring the numerous probe currents. The electronics also have sufficient flexibility to perform various calibrations and functional checks from outside the vacuum chamber to verify measurement accuracy over the 23,000-h duration of the EDU wear test.

At the time of the writing of this paper, the TVD for AEPS has been constructed and installed in GRC's Vacuum Facility 5 (VF5), where a short wear test is currently being performed with a secondary objective of verifying the TVP, TVR, and TVE functionality. Once the TVD has been sufficiently demonstrated, along with other AEPS diagnostics and support hardware, the TVD will be implemented in the 23,000-h wear test of the AEPS EDU.

Diagnostic Design Overview

AEPS Thrust Vector Diagnostic Design Objectives

The objective of the AEPS TVD is to assess the EDU's thrust vector behavior throughout the planned 23,000-hour EDU wear test (Ref. 2). This includes measuring the thruster's beginning of life behavior, the end of life behavior, and any transients or drift throughout the test campaign. More specifically, the TVD will be used to verify that the AEPS requirements related to the thruster's thrust vector are met. Furthermore, in performing these measurements, the TVD must not exceed any AEPS design capabilities, notably the voltage standoff capability in the presence of a facility maximum backsputter rate. After consideration of all AEPS requirements, it was determined that the thrust vector diagnostic design is driven primarily by two AEPS requirements:

1. *The thrust vector offset from the mounting surface normal vector shall not exceed 1.5° over the entire throttling range and over the lifetime of the thruster.*
2. *All thruster components shall maintain the required voltage standoff capability in the presence of a facility carbon backsputter rate of $2 \mu\text{m/kh}$ for 23,000 h.*

These two AEPS requirements led to six thrust vector diagnostic design objectives.

- i. *The diagnostic needs to have sufficient accuracy and resolution to track a thrust vector deviation of 1.5° or less.*
- ii. *The diagnostic needs to provide an absolute thrust vector measurement relative to the thruster's mounting surface normal vector.*
- iii. *The diagnostic needs to survive the test facility environment for at least 23,000 h of thruster operation.*
- iv. *The diagnostic needs to be capable of taking measurements as frequently as every 5 min, when observing transient behaviors.*
- v. *The diagnostic needs to be operable over the EDU thruster's entire throttling range.*
- vi. *Implementation of the diagnostic needs to not increase the facility lifetime average backsputter rate above $2 \mu\text{m/kh}$.*

The first diagnostic design objective necessitates a capability to reliably assess the thrust vector deviations from the thruster mounting surface normal vector of no more than 1.5° over the life of the thruster. The associated thruster requirement is interpreted that any uncertainty in the measurement will result in a reduction in the magnitude of the allowed deviation to ensure compliance. For example, if the uncertainty of the measurement is determined to be $\pm 0.25^\circ$, then the deviation cannot exceed $1.25^\circ \pm 0.25^\circ$. By doing so, confidence shall be high that the thruster requirement is met. Towards that end, significant effort must be made to minimize uncertainties in the thrust vector determination.

The second diagnostic design objective necessitates that the measurement be an absolute measurement relative to the mounting surface normal vector. To achieve an absolute measurement, the diagnostic must have sufficient capability to track not only the probes location and orientation, but its relative position to the mounting surface normal vector.

The third design objective necessitates that the TVP be of sufficiently robust design to survive the full 23,000-h duration of the EDU test. The probe must be resistant to degradation from exposure to the plume, resistant to the accumulation of carbon backsputtered from the chamber surfaces, and capable of withstanding the large temperature and pressure variations within the facility.

The fourth diagnostic design objective necessitates the capability to acquire thrust vector measurements as frequently as every 5 min during anticipated periods of thruster transient behavior. This requirement primarily relates to the transient startup period prior to the thruster reaching thermal steady-state. During this period, deviations in the thrust vector are known to occur as components heat, expand, and shift (Appendix A).

The fifth diagnostic design objective necessitates that the probe be capable of withstanding the rigors of the thruster's plume at maximum discharge current without failure, but also be sensitive enough to perform its function at the thruster's minimum discharge current.

Finally, the sixth diagnostic design objective necessitates that implementation of the diagnostic only minimally increase the backsputter rate of the test facility. The nominal backsputter rate of the test facility is about $1.9 \mu\text{m/kh}$. The AEPS thruster voltage standoff capability is required to be maintained in the presence of a facility backsputter rate of $2 \mu\text{m/kh}$ for 23,000 h. Thus, the thrust vector diagnostic and any other changes to the test facility ahead of the EDU long duration test cannot raise the average backsputter rate by more than $0.1 \mu\text{m/kh}$.

Historic Approaches to EP Thrust Vector Determination

Numerous approaches have historically been pursued to measure the direction of the thrust vector for gridded-ion and Hall-effect thrusters. At the onset of the AEPS project, development of a far-field thrust vector probe was anticipated similar to the one implemented by Polk and Snyder (Refs. 3 to 5). Polk's diagnostic, which characterized the behavior of the NSTAR ion thruster, consisted of a square array of graphite rods, 16 vertical and 16 horizontal, each rod 1.2 m long and 9 mm diameter. GRC has also recently scaled the Polk approach for investigation of NASA's Evolutionary Xenon Thruster-Commercial (NEXT-C) gridded-ion thruster. The GRC version of the probe consists of an 18×18 array of graphite rods, with a diameter of 1.9 cm and a length of 1.52 m (Figure 1). The probe is installed in GRC's Vacuum Facility 16 (VF16) near the opposite end of the vacuum chamber from the thruster. The reason for mounting the probe close to the beam dump, on the opposite end of the chamber from the thruster, is that the probe becomes almost indistinguishable from the graphite beam dump as a source of backsputtered graphite. This location in VF16 results in the captured beam angle at about $\pm 6^\circ$. The closer the probe is situated to the thruster, the larger the total angle of the thruster beam captured by the probe. However, the rate of backsputtered graphite onto the thruster also increases rapidly as the probe is moved closer in proximity to the thruster. Fortunately, given the uniformity and near Gaussian nature of the gridded-ion thruster beam current, $\pm 6^\circ$ is accepted as sufficient to accurately track the beam current centroid. A discussion of the NEXT-C graphite-rod thrust vector diagnostic is included as Appendix A such that the reader can better understand the significant value and simplicity of the approach, and also better understand why the approach was ultimately not pursued for AEPS and deemed not preferred when applied to a Hall-effect thruster in situations where only a limited total angle of the beam is captured.

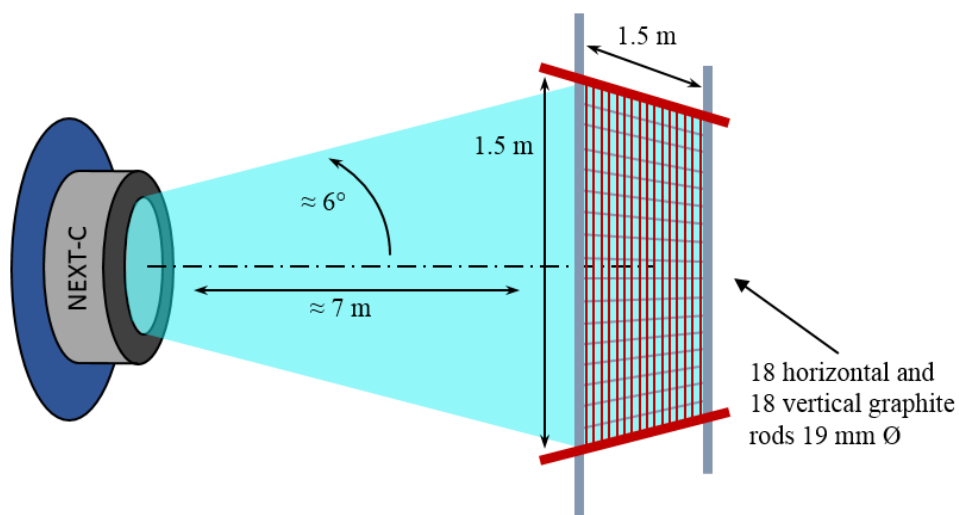


Figure 1.—Schematic of the NEXT-C Thrust Vector Probe as installed in GRC Vacuum Facility 16.

Another thrust vector determination approach by Pollard (Refs. 6 to 8) consists of four double-wire Langmuir probes in the shape of a cross, which is placed downstream in a thruster's plume. Using a motorized positioning system, the instrument is moved horizontally and vertically until the collected currents on the probe wires balance. The location of balanced currents is assumed the beam center. This approach requires an assumption of azimuthal symmetry, as the Langmuir probe wires only measure the beam current of a small fraction of the thruster plume. Pollard also employed a single wire probe to profile the beam of the T5 Ion Engine (Ref. 9).

A direct approach to measuring the thrust vector has been demonstrated by mounting a thruster on a beam with a torsion balance (Refs. 10 and 11). By angling the thruster so that the normal vector of the exit plane of the thruster is parallel to the beam, the lateral component of force can be measured by the torsion balance from the resulting generated moment. Additionally, by changing the angle of the thruster relative to the beam, the axial component of the thrust can be determined. Unlike plasma probes, such a setup provides direct measurement of the thrust vector components. However such an apparatus is challenging to implement. The approach is better suited for experiments dedicated to acquiring thrust vector data, than being an unobtrusive diagnostic element of an already complex test campaign.

An array of retarding potential analyzers (RPAs) has also been implemented to determine the thrust vector of the High Efficiency Multistage Plasma Thruster (HEMPT) (Refs. 12 and 13). In this setup, 37 RPAs are mounted with one every 5° in a 2-m semicircular arc, which can rotate through the entire plume of the thruster. The benefit of using RPAs is that ions solely of selected energy levels can be acquired, allowing for mapping of the different ion energies in the exhaust. A difficulty of using such a setup is that each RPA consists of a series of grids at slightly different orientations, introducing significant uncertainty in their transparency. Thus an array of RPAs requires much care in calibration, as each RPA has unique characteristics. Additionally, the small collection current of an RPA, resulting from the low transparency of multiple stacked grids, requires significant dwell time at each measurement location in the plume. The longer the dwell time, the better the accuracy, but the greater the degradation of the RPA grids, increasing risk of probe failure. The time required to sweep the HEMPT plume is estimated at 15 min (Ref. 12).

Another approach to determining an EP thruster's thrust vector is an array of Faraday probes swept through a plume (Refs. 14 to 17). Faraday probes do not allow for discrimination of ion energies like an RPA, rather they collect all ions. Thus, there is greater concern of facility effects impacting the measurement. However, Faraday probes are comparatively simple in design, and they provide good signal strength while swept rapidly through a plume, reducing the likelihood of probe failure. As shall be discussed, this approach was ultimately determined the most appropriate for the AEPS EDU 23,000-hr wear test.

Analyses Performed to Guide the AEPS TVD Development

Accurate measurement of the thrust magnitude of electric propulsion devices is commonly achieved using a thrust stand with freedom of motion in exactly a single direction of motion. The contribution of off-axis components to the thrust magnitude are typically negligible compared to the axial direction. However, while the magnitude of the thrust off-axis may be small, it may be sufficient to result in nontrivial torques on a spacecraft. Knowledge of the magnitude, speed, and predictable nature of thrust vector deviations from the mounting surface normal vector throughout operation are important inputs for satellite and mission planners. The experimental challenge becomes how to reliably make thrust vector measurements for a particular class of thruster in a ground test facility.

The most desirable method to determine the thrust vector behavior is through direct measurement, requiring few assumptions. However, because off-axis forces are generally quite small and the measurement must be made within vacuum, a direct measurement is very challenging. Apparatus' that have been developed to make such measurement (Refs. 10 and 11) are complex. As a result, most often EP developers favor inferring the thrust vector behavior by indirect measurements. While indirect measurements inherently have a greater degree of uncertainty, they can often be integrated into existing test setups in a minimally intrusive manner. Given the broad scope of the AEPS development, a thrust vector diagnostic employing

indirect measurement was determined most appropriate to provide adequate results within the schedule, within reasonable budget, and while minimally interfering with other test objectives.

In some prior efforts, the thrust vector deviation in a single degree of freedom has been approximated using a single current probe translated in a semicircular arc through the thruster plume. The orthogonal axis is then determined by rotating the thruster 90° and repeating the measurement. For the AEPS test campaign, such manipulation of the thruster is not appropriate. Thus, a multidimensional plume measurement is needed.

In order to achieve a relatively low degree of uncertainty in the thrust vector determination, the assumptions required to correlate the plume measurements with a thrust vector were carefully considered. Assumptions such as azimuthal symmetry, while likely a reasonable assumption for a gridded-ion thruster, were determined inappropriate given the azimuthal nature of a Hall-effect thruster's discharge channel. A minor reduction in mass flow at a single azimuthal location in the discharge channel of a Hall thruster, for example due to debris partially clogging an anode orifice, would result in a significant plume deviation from azimuthal symmetry, which might not be evident and quantifiable on a probe design assuming such symmetry. As such, the probe concepts considered for AEPS were (1) a square array of graphite rods, (2) a swept linear array of Faraday probes, and (3) a swept linear array of RPAs.

Based on prior experience at JPL (Refs. 3 to 5) and GRC (Appendix A) with the graphite rod approach, it was the AEPS development team's initial preference. The probe design had recently been implemented at GRC for the NEXT-C gridded-ion thruster development. Additionally, significant data exists at JPL from prior investigations with gridded-ion thrusters, yielding reasonable confidence in the methodology and reliability of such an apparatus. The static nature of the probe also makes installation and reference to the thruster's mounting surface normal vector straight forward. The primary concerns with the approach were the carbon backscatter rate and the scale of device necessary to collect a sufficiently large percentage of the AEPS thruster's beam. The first issue was easily handled through the use of a facility backscatter model that has been well correlated with measurements within VF5 during thruster operation. The model indicated that a graphite rod style probe would need to be situated approximately 10 m from the thruster to avoid violating the AEPS thruster backscatter capability. This location places the probe immediately in front of the VF5 beam dump. To maximize the area of the beam centroid collected, a probe of approximately 2.5×2.5 m was conceived, which would closely fit within the limitations of the facility. At 10 m distance, this corresponds to a plume collection angle of approximately ±7°. Not too dissimilar to the collection angle of the probe implemented in GRC VF16 as described in Appendix A and schematically illustrated in Figure 1.

Faraday probe beam current data (±90° of beam center, 1/8° steps) collected with the HERMeS Technology Demonstration Unit 1 (TDU-1) operating in Vacuum Facility 6 (VF6) was acquired (Figure 2) and analyzed to help determine whether ±7° was sufficient to verify the AEPS thrust vector requirement. While determination of a gridded-ion thruster's beam center by fitting data from a limited collection angle has been deemed acceptable, it is not immediately obvious if a similar conclusion can be reached for Hall-effect thrusters. While gridded-ion thrusters result in a reasonably clean beam with a Gaussian profile, the azimuthal discharge channel of a Hall-effect thruster results in a centerline inflection in the beam current density as shown in Figure 2. The TDU-1 data was collected by sweeping a single Faraday probe through the TDU-1 plume in a semicircular arc at various radial distances.

Figure 3 illustrates one reason why the centroid of a Hall thruster is particularly troublesome for determination of beam center, and by correlation thrust vector direction. A Gaussian profile is a poor fit to the TDU-1 data. The beam current inflection near centerline dissuades use of a simple Gaussian fit. As a workaround, selective exclusion of the beam center inflection data was attempted to achieve a qualitatively better fit. In Figure 4, the data is fit with a Gaussian profile, however the data between the inflection points of the Hall thruster beam current of ±3° is excluded. The outcome is a qualitatively reasonable fit to the larger beam profile. However, it is not yet clear whether a Gaussian profile is appropriate for fitting Hall-thruster plume current data, or whether excluding data between ±3° results in a quantitatively better determination of thrust vector direction.

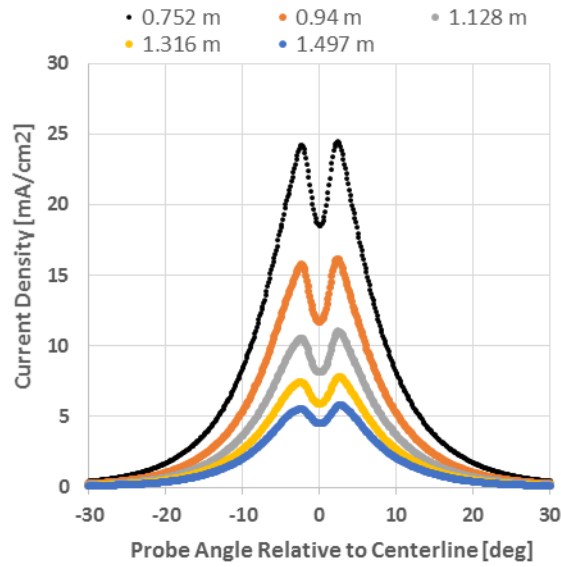


Figure 2.—TDU-1 Faraday probe beam current density measurements in VF6.

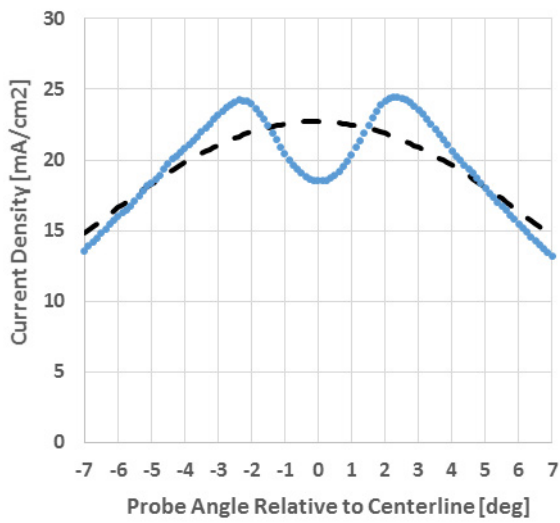


Figure 3.—Gaussian fit to 0.75 m TDU-1 Faraday probe data between $\pm 7^\circ$.

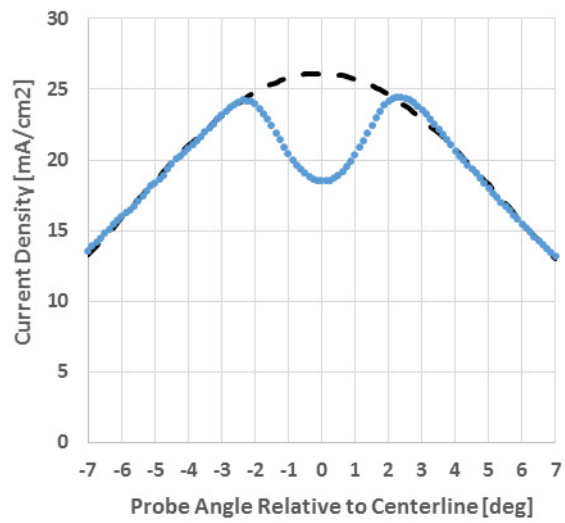


Figure 4.—Gaussian fit to 0.75 m TDU-1 Faraday probe data between $\pm 7^\circ$, excluding data between $\pm 3^\circ$.

To qualitatively demonstrate whether a Gaussian profile is appropriate for fitting Hall-thruster plume current data, a larger dataset between $\pm 30^\circ$ was considered, both including (Figure 5) and excluding (Figure 6) data $\pm 3^\circ$ off the plume centerline. For the nominal 12.5 kW TDU-1 operating condition, a collection angle of $\pm 30^\circ$ encompasses nearly all thrust contributing ions. Based on the fits shown in Figure 5 and Figure 6, a Gaussian profile, whether including or excluding the centerline inflection does not qualitatively well match the data. In fact, excluding $\pm 3^\circ$ does not result in any noticeable difference in fit quality. Before proceeding to quantitatively determine whether $\pm 7^\circ$, as anticipated with a graphite rod TVD in VF5, is sufficient for locating beam center, a fitting profile that qualitatively better fits the full TDU-1 beam current data was sought. Two additional fitting profiles were considered, a Lorentzian and a pseudo-Voigt.

The Gaussian, Lorentzian, and pseudo-Voigt profiles are described by the following equations,

$$\text{Gaussian: } G(\theta) = a_1 e^{-(\theta-\theta_0)^2/b} \quad (1)$$

$$\text{Lorentzian: } L(\theta) = \frac{a_2}{(\theta-\theta_0)^2+c} \quad (2)$$

$$\text{Pseudo-Voigt: } V(\theta) = G(\theta)L(\theta) = \frac{ae^{-\frac{(\theta-\theta_0)^2}{b}}}{(\theta-\theta_0)^2+c} \quad (3)$$

where a , a_1 , a_2 , b , and c are fitting constants, θ is the arbitrary probe angle and θ_0 is the location of beam center. The pseudo-Voigt is a simple product of the Gaussian and Lorentzian profiles, rather than a true convolution. Figure 7 illustrates that regardless of the fitting profile, a Hall thruster's beam current density cannot be easily fit while including the full beam current density dataset. However, as shown in Figure 8, by excluding the data associated with the inflection in the beam current data, the Lorentzian fits the data reasonably well except for over-predicting slightly in the wings and the pseudo-Voigt fits so well as to be nearly indiscernible from the dataset.

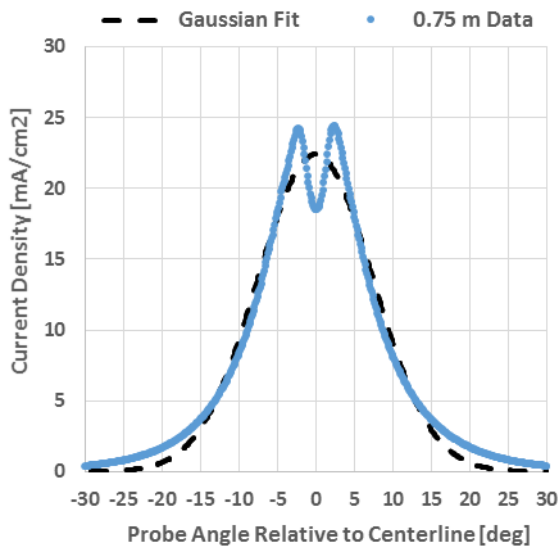


Figure 5.—Gaussian fit to 0.75 m TDU-1 Faraday probe data between $\pm 30^\circ$.

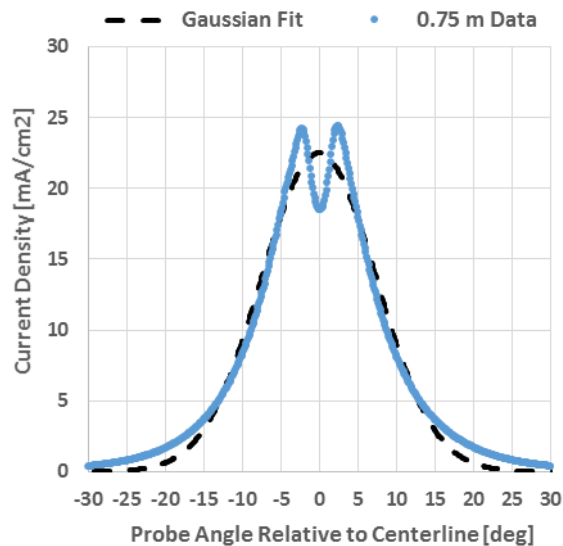


Figure 6.—Gaussian fit to 0.75 m TDU-1 Faraday probe data between $\pm 30^\circ$, excluding data between $\pm 3^\circ$.

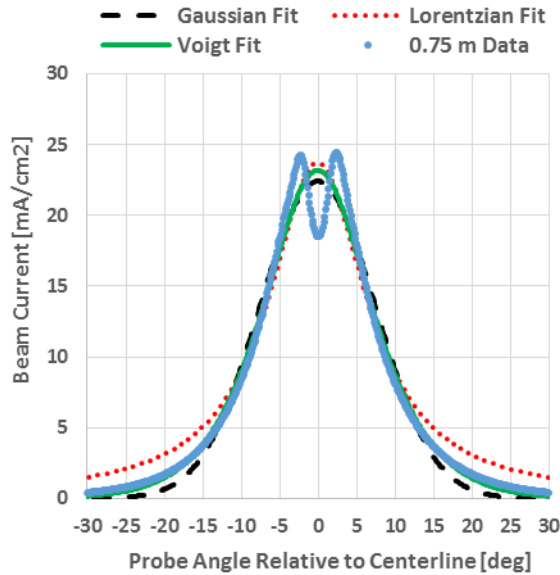


Figure 7.—Gaussian, Lorentzian and pseudo-Voigt fit to 0.75 m TDU-1 Faraday probe data between $\pm 30^\circ$.

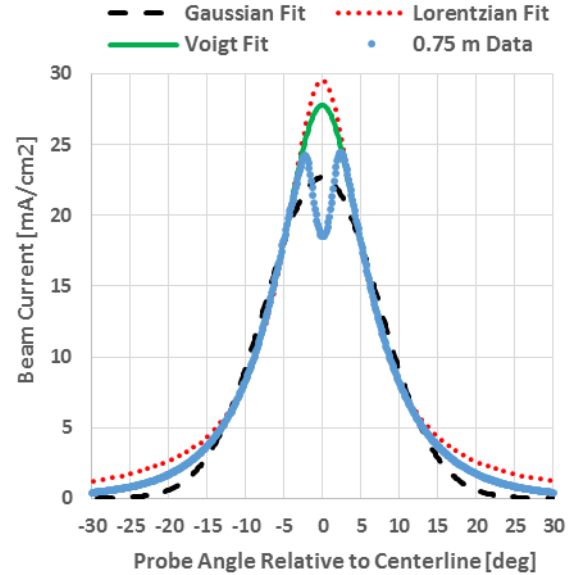


Figure 8.—Gaussian, Lorentzian and pseudo-Voigt fit to 0.75 m TDU-1 Faraday probe data between $\pm 30^\circ$, excluding data between $\pm 3^\circ$.

TABLE 1.—DISCREPANCIES BETWEEN CENTERLINE AS DETERMINED BY VARIOUS PROFILE FITS AND KNOWN BEAM CENTER FOR A TDU-1 FARADAY PROBE DATASET BETWEEN $+5^\circ$ AND -9° , INCLUDING AND EXCLUDING THE CENTERLINE INFLECTION

| $\pm 3^\circ$ | Resulting fitting error, deg | | |
|---------------|------------------------------|------------|---------|
| | Gaussian | Lorentzian | p-Voigt |
| Including | 0.436 | 0.523 | 0.436 |
| Excluding | 0.048 | 0.041 | 0.035 |

Having qualitatively identified a better profile by which to fit AEPS Hall thruster beam current density data, further consideration is given to quantitatively demonstrating if any of the described fitting profiles provide more reliable determination of beam center using a limited dataset between $\pm 7^\circ$. Furthermore, because a graphite rod TVD is anticipated to be stationary, and thrust vector deviations as large as 1.5° are permissible under the AEPS requirements, rather than fitting a symmetric dataset between $+7^\circ$ and -7° , the dataset is fit between $+5^\circ$ and -9° . Fitting asymmetric datasets can cause havoc on fit quality, thus is the more conservative approach to quantitatively demonstrating if one of the fitting profiles is more accurate at locating beam center. Table 1 summarizes the error resulting from each fit for this specific TDU-1 dataset. Error was calculated as the difference between the regression beam center parameter θ_0 and the beam center as determined by numerical integration of the complete dataset. In each case, the fit quality is maximized using a least squares fitting methodology.

Approximately a half-degree of error is incurred by fitting the full asymmetric dataset (Figure 9), regardless of profile choice. On the other hand, exclusion of the data within the region of inflection proves considerably more accurate for all profiles considered (Figure 10). The pseudo-Voigt is marginally more accurate than either the Gaussian or Lorentzian fits at locating beam center. The pseudo-Voigt is also a better quality fit to the dataset.

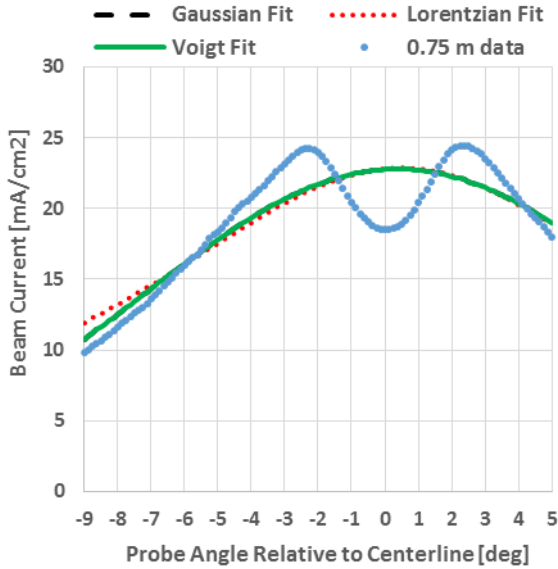


Figure 9.—Various fits to 0.75 m TDU-1 Faraday probe data between +5° and -9°.

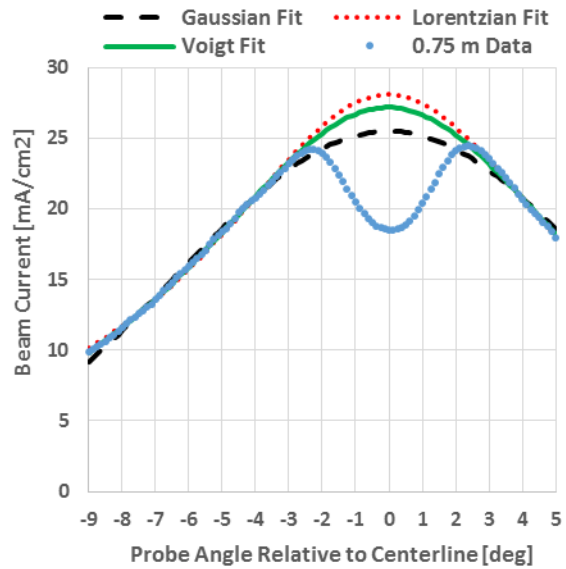


Figure 10.—Various fits to 0.75 m TDU-1 Faraday probe data between +5° and -9°, excluding data between ±3°.

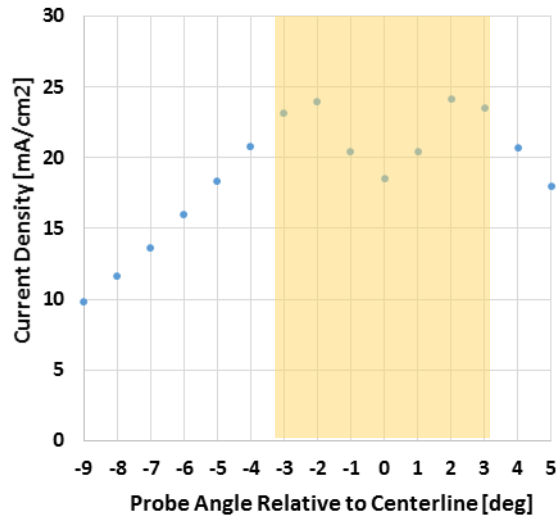


Figure 11.—0.75 m TDU1 Faraday probe data between +5° and -9° (1 data point per degree).

While not rigorously proven, given that only a single TDU-1 dataset is considered here, a pseudo-Voigt fit appears a reasonable choice for fitting AEPS Hall thruster beam current density data, when excluding data within the region of inflection near centerline. However, it is still unclear if $\pm 7^\circ$ is sufficient scale for a Hall-effect thruster TVD based on graphite rods or other discretely spaced probes. The Faraday probe data considered here is particularly dense with data collected every $1/8^\circ$. However, a graphite rod approach similar to the NEXT-C TVD would yield approximately 1 beam current measurement per degree between $\pm 7^\circ$ with the TVD located at the far end of VF5. To illustrate, Figure 11 provides data from the TDU-1 sample dataset between $-9/+5^\circ$ with 1° spacing. If the data between $\pm 3^\circ$ is excluded from the pseudo-Voigt fit, nearly 50 percent of the captured plume angle is discounted, leaving only 8 data points remaining. Fitting such a limited dataset across a limited beam angle poses significant risk to achieving a highly accurate determination of beam center. A further problem when considering

such a limited dataset is objectively identifying the beam centerline inflection points, which may become confused by variations in measurement error between the individual probes. The sample NEXT-C graphite rod TVD data in Appendix A (Figure 27) illustrates anticipated variations in measurement error compared against an expected Gaussian beam profile. The probe-to-probe variation in measurement error is largely the result of characteristic differences between each graphite rod (cross-sectional area, roughness, density, etc.). Based on this analysis, a graphite rod TVD approach for the AEPS EDU wear test is anticipated to offer insufficient accuracy to verify that the thrust vector requirement is met.

While a stationary graphite rod array TVD was deemed not appropriate for AEPS, a probe array based on either Faraday probes or RPAs sweeping through the plume in a semicircular arc is still viable. Since a mobile probe array only crosses through the thruster beam while acquiring periodic measurements, it has limited impact on the average rate of material backspattered toward the thruster. As such, rather than the probe situated 10 m from the thruster face, the probe can interrogate the plume in relative close proximity to the thruster. For example, while a 2.5-m tall probe at 10-m distance captures about $\pm 7^\circ$ of the plume, a 0.5-m tall probe at 1-m can capture about $\pm 14^\circ$. By interrogating a significantly larger portion of the plume, exclusion of $\pm 3^\circ$ will have significantly less of a delirious effect on the accuracy of beam center determination. Furthermore, by being in closer proximity to the thruster, the measurement will be less subject to facility effects such as charge exchange and beam bending due to pressure gradients. The smaller TVD also has the benefit of being easier to construct and install.

A linear array of Faraday or RPA probes is now considered, but in closer proximity to the thruster face, where facility scale is no longer a limiting factor on the maximum beam angle that can be interrogated. A probe scale capable of capturing $\pm 15^\circ$ is now considered. Figure 12 shows fits to the sample TDU-1 Faraday probe beam current density dataset between $+13^\circ$ and -17° , while Figure 13 shows the same dataset and fits, but excluding $\pm 3^\circ$. Table 2 summarizes the beam center error resulting from each fit for this specific dataset and angular limits.

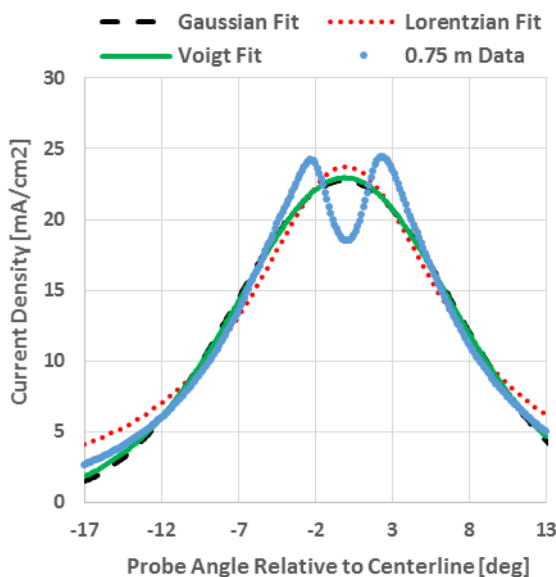


Figure 12.—Various fits to 0.75 m TDU-1 Faraday probe data between $+13^\circ$ and -17° .

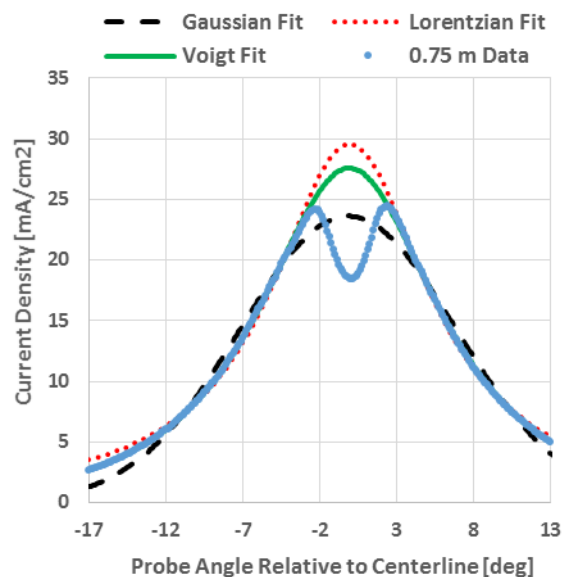


Figure 13.—Various fits to 0.75 m TDU-1 Faraday probe data between $+13^\circ$ and -17° , excluding data between $\pm 3^\circ$.

TABLE 2.—DISCREPANCIES BETWEEN CENTERLINE AS DETERMINED BY VARIOUS PROFILE FITS AND KNOWN BEAM CENTER FOR A TDU-1 FARADAY PROBE DATASET BETWEEN +13° AND -17°, INCLUDING AND EXCLUDING THE CENTERLINE INFLECTION

| ±3° | Resulting fitting error, deg | | |
|-----------|------------------------------|------------|---------|
| | Gaussian | Lorentzian | p-Voigt |
| Including | -0.061 | 0.048 | -0.042 |
| Excluding | -0.072 | 0.019 | -0.006 |

Whether, including or excluding the data within the inflection region of the beam current, fitting a larger angular fraction of the thruster plume eliminated most of the calculated error. Although, the best beam center determination and fit quality still result from the pseudo-Voigt profile fit excluding ±3° as shown in Figure 13.

While exclusion of the Hall thruster beam center inflection for this analysis has thus far proven educational, subjective manipulation of the data by exclusion of the beam center inflection is not consistent with rigorous data analysis and verification of AEPS requirements. The subjective bias implicit in such a data processing methodology could result in inconsistent determination of whether the thrust vector requirement has been met. Rather than implementing a subjective data exclusion methodology during data post-processing in an attempt to improve beam center determination accuracy, a data weighting scheme was devised.

To help understand how the weighting method implemented was determined, Figure 14 schematically shows a single current probe translating through a beam of ions, collecting ion current data at discrete locations. Making the assumptions that all ions within a discrete region of the hemispherical plume are traveling with the same velocity, and all ions are singularly ionized, the thrust contribution by ions traveling through a specific region, dA , can be approximated by

$$dT \propto jdA \quad (4)$$

where j is the beam current density. In other words, the thrust contribution, dT , is proportional to the ion flux through the discrete area, dA . This leads to the observation that as the beam angle approaches centerline, and dA approaches zero, the thrust contribution also approaches zero. Figure 15 shows that by weighting each beam current measurement by the associated hemispherical beam area to approximate contribution to overall thrust, that beam center is conveniently not a major contributor to overall thrust. Thus, the beam center inflection, which causes issues with fitting standard profiles, can be logically discounted as it physically represents a minor contribution to the overall thrust. Conversely, at larger beam angles, while the magnitude of the beam current density falls, the representative cross sectional region and associated thrust contribution grows. For the beam current dataset considered, the beam current density measurement representing the largest flux of ions occurs at approximately 6°.

The hemispherical area represented by each probe measurement can be approximated by

$$dA \propto rd\theta \quad (5)$$

where $r = R \sin \theta$, R is the probe distance from the center of the thruster face, and $d\theta$ the step angle.

Then,

$$dA \propto R \sin \theta d\theta \quad (6)$$

If probe scans hold R and $d\theta$ constant,

$$dA \propto \sin \theta \quad (7)$$

Thus, the beam current density measurements may be weighted by $\sin \theta$ to reflect contribution to thrust. Since the beam angle is not known a priori, the weighting method must be performed iteratively in combination with the beam profile fitting.

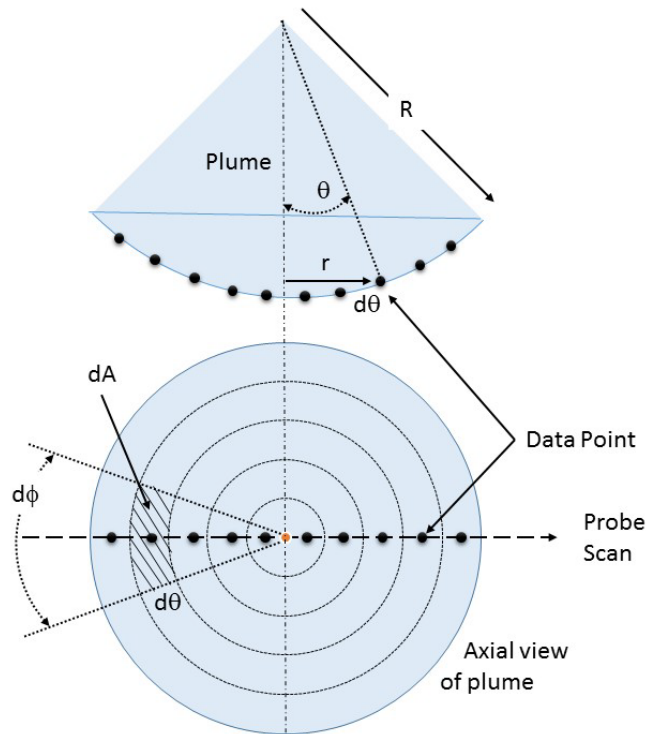


Figure 14.—Schematic showing the weighted significance of current density measurements throughout the sweep of a plume. Measurements at high angles represent greater cross-sectional regions of the plume.

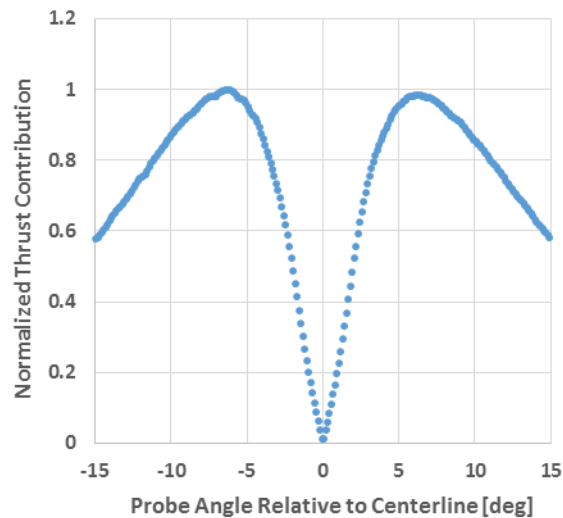


Figure 15.—Normalized 0.75 m TDU-1 Faraday probe data between ± 15 , which has been weighted by the hemispherical area associated with each beam current measurement to approximate thrust contribution.

To further simplify the data processing, rather than weighing the data and employing a least-square fit, minimizing

$$\sum_{i=1}^n r_i^2 \quad (8)$$

where r_i is the residual $r_i = y_i - V(\theta_i)$, the same result can be achieved by simply weighting the residual. This approach has the benefit of preserving the beam current raw data while performing the data processing and only manipulate the fit. Thus, Equation (3) shall be fit by minimizing $\sum_{i=1}^n (r_i \sin(\theta - \theta_0))^2$, while iteratively solving constants a, b, c, θ_0 . The value found for θ_0 is the estimated beam deviation from the mounting surface normal vector within the plane probed. This technique will be referred to herein as a sine weighted residual (SWR).

The resulting error for fits performed to the TDU-1 beam current dataset (no data excluded) using the SWR method for both between $+5^\circ$ and -9° (Figure 16) and $+13^\circ$ and -17° (Figure 17) is summarized in Table 3. The described analysis again predicts the most reliable fit using the pseudo-Voigt profile. However, these fits are now accomplished without subjective exclusion of beam current data. For the case of TVDs with limited angular beam current datasets, while accuracy will decrease by not capturing a significant percentage of the plume wings, a pseudo-Voigt fit using a SWR technique will provide improved accuracy over a Gaussian least-square fit as commonly implemented when interpreting gridded-ion thruster data.

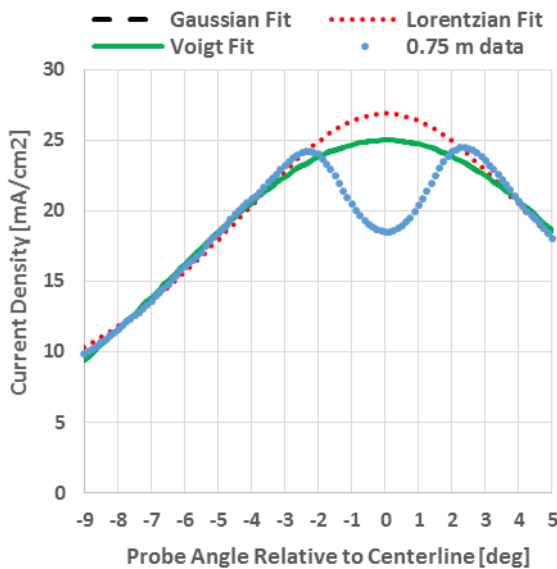


Figure 16.—Various fits to 0.75 m TDU-1 Faraday probe data between $+5^\circ$ and -9° , using a SWR least-square fitting method.

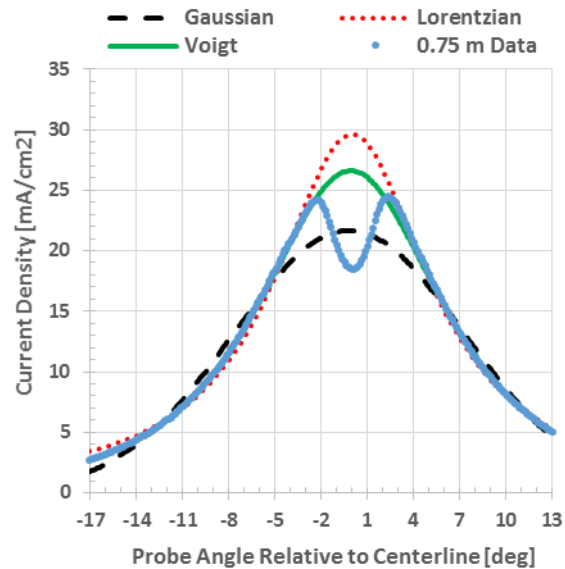


Figure 17.—Various fits to 0.75 m TDU-1 Faraday probe data between $+13^\circ$ and -17° , using a SWR least-square fitting method.

TABLE 3.—DISCREPANCIES BETWEEN CENTERLINE AS DETERMINED BY VARIOUS PROFILE FITS AND KNOWN BEAM CENTER FOR A TDU-1 FARADAY PROBE DATASET, USING A SWR LEAST-SQUARE FITTING METHOD

| Probe Size | Resulting fitting error, deg | | |
|----------------|------------------------------|------------|---------|
| | Gaussian | Lorentzian | p-Voigt |
| $\pm 7^\circ$ | 0.082 | 0.077 | 0.082 |
| $\pm 15^\circ$ | -0.146 | 0.036 | -0.022 |

The outcome of this analysis, based on satisfying the AEPS thrust vector requirement within the constraints of the VF5 test facility, is that:

- While a square array of graphite rods could be a reasonable approach in closer proximity to the thruster, the large probe scale of 2.5×2.5 m and limited beam collection angle of approximately $\pm 7^\circ$, due to the necessity to place the probe 10 m from the thruster to avoid violating the thruster backscatter capability, discourages it as a solution for the AEPS EDU long duration wear test.
- The most reasonable approaches to meet the TVD design objectives are either a linear array of Faraday or RPA probes swept through the plume with a minimum beam collection angle of $\pm 15^\circ$.

An RPA has the notable benefit that one can filter out low energy charge exchange ions, which might erroneously result in the appearance of a thrust vector deviation. The primary downside of the RPA are long dwell times, probe complexity, probe cost, and a high risk of failure over 23,000 h of testing due to internal erosion during dwell.

Thus, the AEPS team concluded that the most appropriate diagnostic for verification of the AEPS thrust vector requirement within the available schedule and budget was a linear array of Faraday probes with a minimum of $\pm 15^\circ$ collection angle. The Faraday probe design follows best practices as outlined by Huang (Ref. 18), including molybdenum collectors and guard rings to limit degradation while traversing the plume.

Design

The design of the Thrust Vector Diagnostic (TVD) consists of three main components: the Thrust Vector Probe (TVP)—an array of Faraday probes, the Thrust Vector Reference (TVR)—the alignment system, and the Thrust Vector Electronics (TVE) package. These components are discussed in the sections that follow.

TVP Design

The chosen design is an array of 23 Faraday probes mounted at 1-m radius on a light-weight aluminum framework, as shown in Figure 18(a). The Faraday probes, Figure 18(b), are positioned every 2° along the arc, from -22° to $+22^\circ$, and the arc is shielded with Grafoil to reduce backscatter, protect the aluminum framework and protect the wiring. Each Faraday probe is mounted such that its collector surface normal vector is oriented toward the nominal thruster center point. Each Faraday probe guard ring and collector are biased to -30 V in operation to reject electrons. The TVP is attached to a probe arm assembly in VF-5, which is connected to an Aerotech Pro225 linear stage (<20 μm resolution) and an Aerotech AGR200 rotary stage (<20 arc sec resolution), allowing for sweeping the thruster plume periodically at a rate of 2 deg/s.

The mounted TVP and VF5 probe package (used for standard plume measurements) are shown in Figure 18(c), and a top view of the TVP relative to the probe package is shown schematically in Figure 18(d). The TVP is tilted at an angle of 7.5° horizontally such that the arc center is located at the nominal thruster center during the sweep. When not in use, the TVP is stored behind the thruster discharge exit plane.

TVE Design

The TVP is connected to the TVE by a 60 conductor wire harness, consisting of five C8132 cables (12 conductor, twisted shielded pairs), with all shields tied at the vacuum facility feedthrough. Measurement of the Faraday probes is performed using circuits containing 100 Ω shunt resistors connected to two NI USB-6363 data acquisition (DAQ) units. The circuit also includes over-voltage protection to mitigate risk of damage to either DAQ. Additionally, type-K thermocouples are placed on the probe array and tilt sensors to track the TVP temperature.

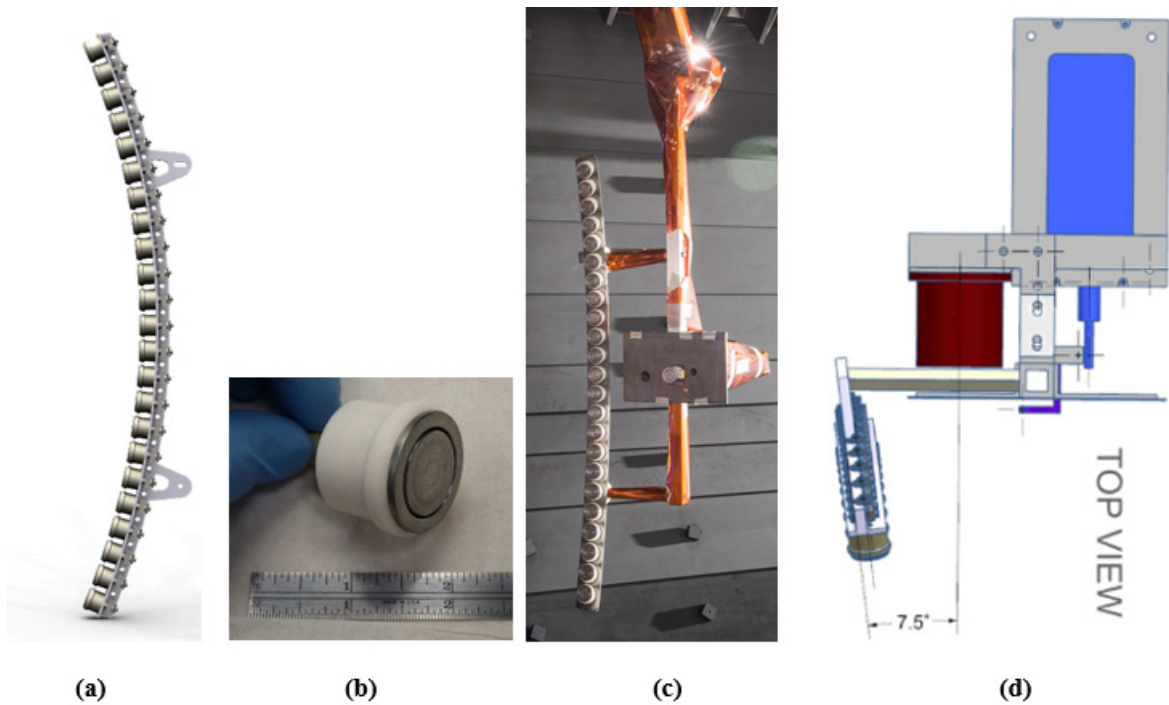


Figure 18.—(a) TVP CAD model. (b) Individual Faraday probe. (c) TVP mounted in chamber with probe package (before Grafoil overlay). (d) Top view of CAD drawing showing TVP relative to probe package.

TVR Design

To properly validate the thrust vector requirement relative to the thruster mounting surface normal vector, a target reference system locates the thruster’s mounting surface normal vector, which is compared against the TVP location. In-situ verification of the absolute alignment of the probe relative to the thruster is possible by an optical alignment system, discussed below. The absolute alignment is conducted at a single location directly in front of the thruster, while the thruster is nonoperational. After which, the rotation stage encoders and tilt sensors locate the probe throughout the rest of its sweep.

Before further discussion of the alignment measurements, a brief description of the coordinate system used in this analysis. The probe coordinate system is located with the origin at the intersection of the cathode centerline and the plane of the inner front pole cover (Figure 19). The rectangular coordinate system is oriented with x pointing opposite to gravity; z pointing in the horizontal component of the mounting structure normal vector, as defined by the mounting structure optical alignment assembly, and pointing towards the thruster beam dump; and y pointing in a direction to satisfy the right-hand rule. The spherical coordinate system is based on the rectangular system with a fixed radius of 1 m, a polar angle (ϕ) measured from the x-axis zenith direction, and an azimuthal angle (θ) measured from the z-axis direction, as shown in Figure 19. The azimuthal angle (θ) increases in the clock-wise direction when viewed from above.

The optical alignment system consists of a precision machined stainless steel tube of 0.29 m end-to-end length and two 795-series Brunson optical reticle targets that were press-fit to both ends of the pipe. These optical targets have reticles that, when looking through the pipe, allow for determining the vector of the pipe relative to the viewer. This pipe is then attached to the thruster mounting plate, defining the mounting surface normal vector. Looking down the pipe and measuring the radial offset between the two optical targets, and also knowing that the two crosshairs are 0.28 m apart, the mounting surface normal vector is calculated. A mechanical shutter is replaced when the alignment tool is not in use to prevent contamination of the targets during thruster firing. This pipe and corresponding optical targets are shown in Figure 20 (shutter system not shown).

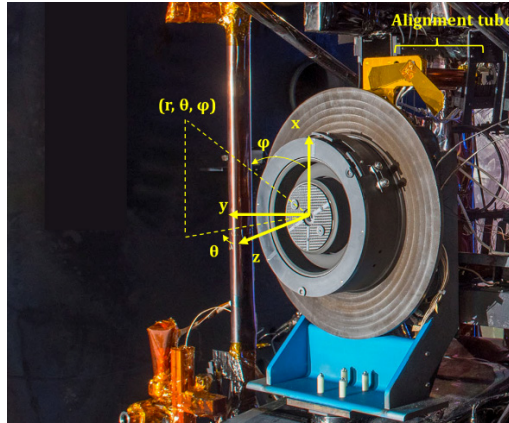


Figure 19.—Probe coordinate systems.



Figure 20.—Target vector reference pipe with optical targets visible.

To locate these optical targets while the vacuum facility is under vacuum, an alignment telescope with a built-in camera is placed at a viewport directly downstream of the thruster. The telescope is leveled and placed in-line with the two reticle targets on the mounting structure assembly. By lining up the telescope with the targets, the mounting normal vector can be ascertained periodically throughout testing. Additionally, a small alignment pin was placed on the TVP arm, which allows for checking whether the TVP arm drifted relative to the crosshairs of the optics targets. The probe assembly is then positioned to a pre-determined theta position to verify the location of the alignment pin with respect to the line created by the mounting structure alignment assembly. To aid in the sighting of the alignment features, an indirectly illuminated Teflon backdrop is used behind the pipe and targets. The shutter and backdrop lights are electrically isolated from the thruster with ceramic standoffs. The telescope and alignment pin are shown in Figure 21.

A demonstration of the in-situ alignment verification is shown in Figure 22. The center image of the figure shows the optical home of the probe, at which point the probe alignment pin is in alignment with the mounting structure alignment assembly. The other four images, from left to right, are $+0.2^\circ$, $+0.1^\circ$, -0.1° , and -0.2° from the optical home. A vertical red arrow is included in Figure 22 to aid in identification of the probe alignment pin. The probe angular resolution of the images in Figure 22 is roughly 0.01° per pixel. The width of the probe alignment pin is approximately 0.1° , which results in a nominal resolution alignment uncertainty of 0.05° for the system. The in-situ alignment system is capable of tracking shifts in both the θ and ϕ direction. Pumping down the facility to vacuum did not lead to a measurable displacement of the probe alignment pin with respect to the mounting structure alignment assembly.

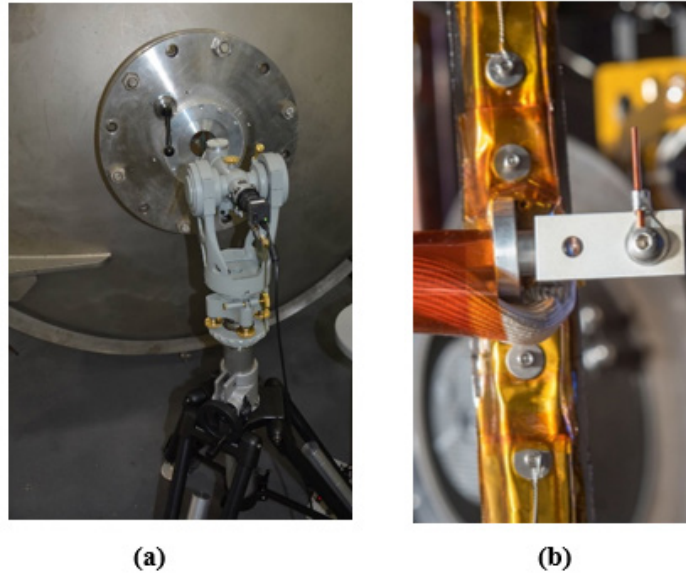


Figure 21.—(a) Brunson alignment telescope located by view-port directly downstream of thruster. (b) Alignment pin on thrust vector probe assembly.

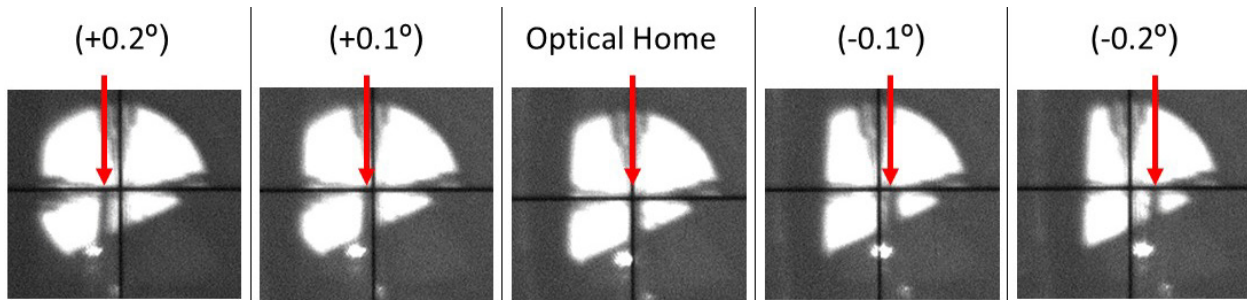


Figure 22.—Optical alignment system demonstration.

Further alignment tracking of the probe assembly is made possible by a series of high resolution gravity referenced inclinometers, Spectron CG-10N electrolytic tilt sensors (1 mV/arc sec sensitivity). While the inclinometer system is not able to provide absolute alignment reference like the optical system, it is able to provide a relative reference for the full sweep of the probe. Figure 23 provides a sketch of the location and orientation of the three inclinometers. Inclinometer I is mounted on the main horizontal member of the probe arm and tracks deviations from horizontal as the probe is swept over its full scan. Inclinometer II is installed to make the same measurement as Inclinometer I but is mounted on the vertical member which supports the TVP. Figure 23(a) provides a view of the thruster from $\theta = 0^\circ$ and $\phi = 90^\circ$ with the probe arm at $\theta = -90^\circ$, such that inclinometers I and II polarity can be described. Inclinometer III was set up to be nominally orientated 90° out of phase with inclinometers I and II. Figure 23(b), provides the same view of the thruster with the probe arm now placed at $\theta = 0^\circ$, such that inclinometer III polarity can be described. Example traces of the three inclinometers are shown in Figure 24. The raw data is shown by circular symbols in Figure 24(a). Regression sinusoidal curves were fit to the inclinometer signals, with the assumption of symmetry at $\theta + 180^\circ$ and -180° . The curve fits are shown in Figure 24(a) with solid lines. The curve fits are background subtracted to remove the arbitrary mounting inclination of the sensors, shown in Figure 24(b). The final background subtracted results of the inclinometers are used to determine the probe arm rotation axis. The phase and amplitude of any of the three inclinometers tracks with the θ and ϕ orientation of the rotation axis of the arm, respectively.

The rotation axis of the probe arm is shown schematically as the orange vector in Figure 23, ideally the rotation axis is coincident with the x-axis but in practice it will deviate. The profiles in Figure 24(b) indicate the probe rotation axis to be $\theta = -50^\circ$ and $\varphi = 1.1^\circ$, which corresponds to a rotation axis of $[0.999, -0.015, 0.012]$. In future work this rotation axis will be used to track changes in the system and correct probe data for tilt.

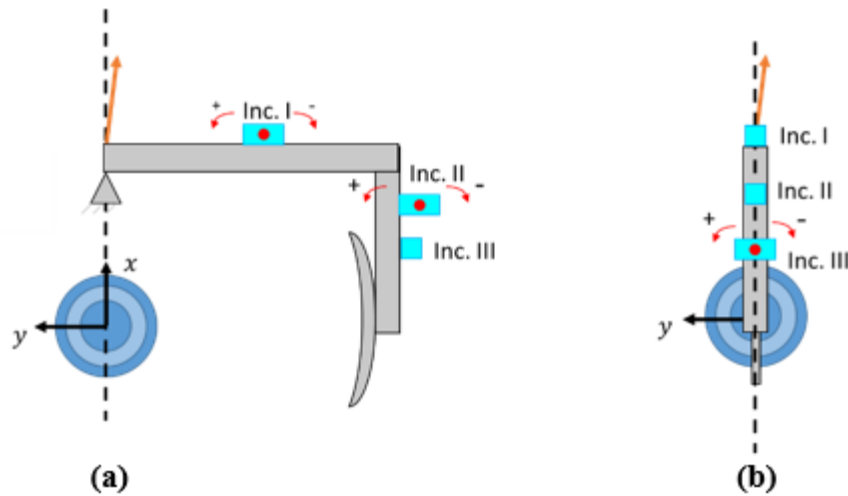


Figure 23.—Schematic of inclinometer orientation and polarity with respect to probe arm assembly with probe arm at (a) $\theta = -90^\circ$ (b) $\theta = 0^\circ$. Inclinometers sketched in teal with red dot indicating inclination axis and arrows indicating polarity. View of thruster sketched from 0° theta.

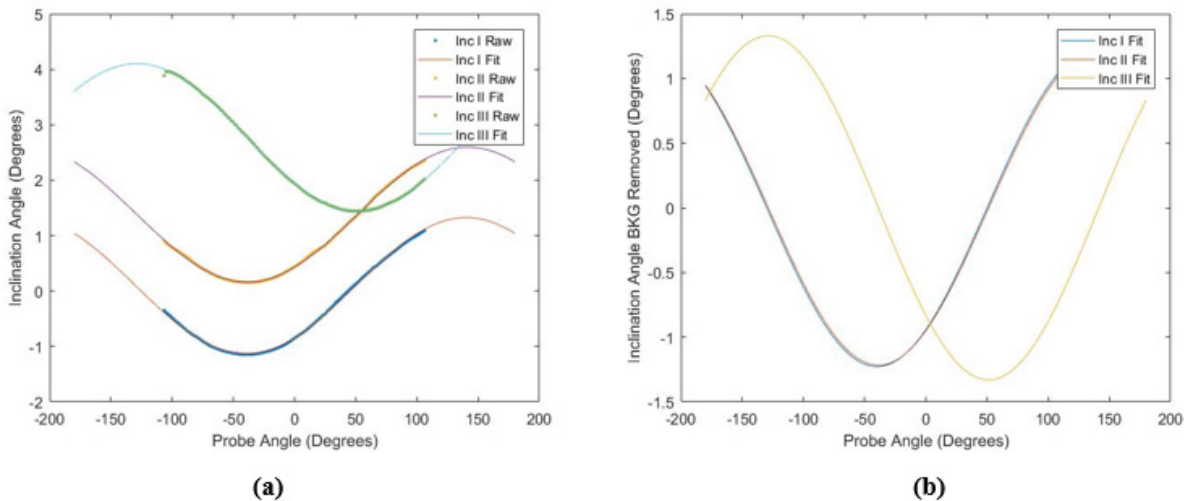


Figure 24.—Inclinometer example traces. (a) Raw traces with curve fits. (b) Background subtracted curve fits used for determination of rotation axis of probe assembly.

Initial Diagnostic Measurements

Initial measurements using the TVD on the TDU-3 have been conducted with the thruster at different operating conditions. Results are currently being analyzed, but initial findings indicate successful measurement of the thruster plume. A sample set of data is shown below in Figure 25. Figure 25(a) through (c) show contour plots created from the beam current density measurements at discharge voltages of 300, 400, and 600 V, respectively. Note that “probe angle” refers to the mounting angle of an individual Faraday probe, and “sweep angle” refers to the angle at which the Faraday probes pass through the thruster plume. A 3D plot of the Faraday probe raw data at 600 V is also shown in Figure 25(d). From these plots, it is shown that the plume has smaller divergence with the thruster at 600 V than at 300 V, as expected. Much of the nonsmooth variations in the contours of this dataset are not representative of the actual plume, but result from instrumentation calibration error. These calibration errors are being mitigated through improvements to the TVE prior to the EDU long-duration wear test.

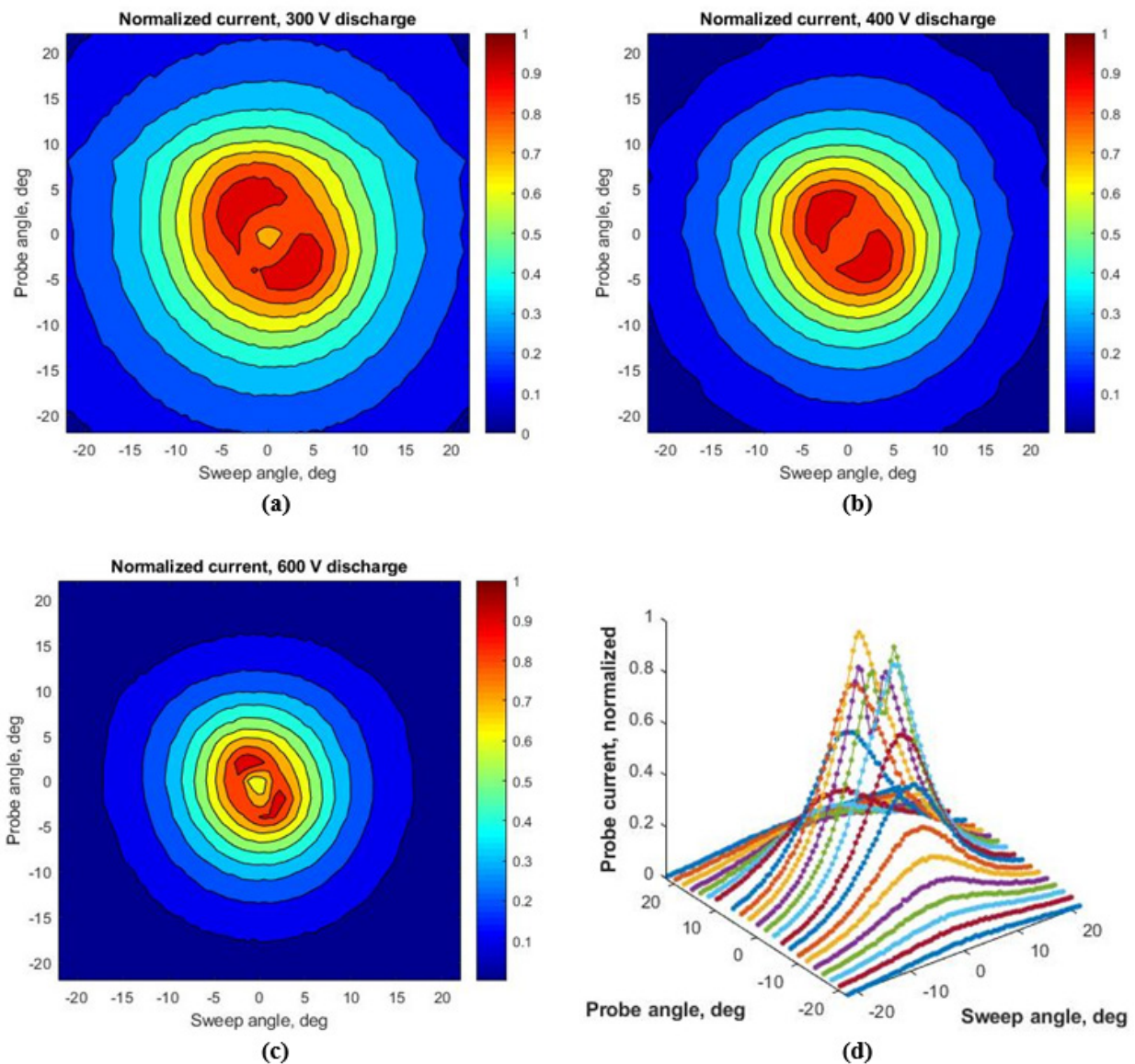


Figure 25.—Contour plots of TDU-3 TVD data in VF-5 at (a) 300 V, (b) 400 V, and (c) 600 V; (d) a 3D plot of Faraday probe raw data at 600 V.

There are several avenues of ongoing work. Initial measurements of the alignment angle have been taken, however work is ongoing for creating the data fitting and processing routines, which will compute the thrust vector deviation. Additionally, the slight asymmetry in the contour plots may be due to the tilt of the TVP as it passes through the thruster plume: the tilt sensor data is presently being incorporated into the data processing routines. Determining whether the TVP arm has drifted throughout the test operation will be examined later with further measurements of the alignment. Additionally, the TVD is planned to be run with the TDU-3 thruster in the near future while performing a thruster cold start, which will provide information on how the thrust vector changes while the thruster warms up. A thrust vector determination uncertainty analysis is being performed for the AEPS TVD as built.

Conclusion

The TVD design presented here is the result of an analysis of various potential thrust vector determination techniques. An array of 23 Faraday probes swept through the plume is determined the most appropriate technique to verify the AEPS thrust vector requirement within the available schedule and budget. The TVD has been fabricated, installed in the GRC Vacuum Facility 5, and successfully operated during a thruster test. Initial analysis of the results show expected behaviors as thruster discharge voltage is varied. Future work includes incorporating the tilt sensor data into the results, verifying thruster alignment, completing the data processing routines, completing the uncertainty analysis, and operating the TVD across the full thruster operating range and during expected transients such as thruster warm-up.

Appendix A.—GRC NEXT-C Thrust Vector Diagnostic

Background

Thrust vector characterization tests have recently been completed on a prototype-model ion engine at NASA Glenn Research Center (GRC). The tests were completed to: (a) define requirements for flight thruster acceptance tests; and (b) ensure the flight gimbal design can sufficiently null disturbances produced by thrust vector offsets from the spacecraft center of mass. Prior to completing the tests, a literature search was performed to investigate the different schemes used to characterize the thrust vector. Tests have historically consisted of using a 2-D array of electrostatic probes to map the beam current, and then defining the measured beam centroid as the thrust vector offset. This work has been completed with Faraday probes, double Langmuir probes, and far-field cylindrical rods (Refs. 4, 7, 19 to 21). The far-field cylindrical rod approach was successfully used during an 8000 h wear test with the NSTAR engine, and was baselined for the NEXT engine. An ion beamlet model was used to estimate the collected rod currents as a function of thruster operating condition, rod length, and axial distance from the thruster. These calculations led to the design of the thrust vector probe array, as described in the following section. The following sections will summarize data that has been obtained with a prototype engine, and a more comprehensive report will be published in the near future (including data from multiple NEXT engines).

Apparatus

Tests were conducted using the Dev-C thruster, which is a slightly modified version of the prototype PM1R engine (Refs. 22 and 23). The thruster utilizes a ring-cusp discharge chamber with a conical upstream segment and a cylindrical downstream portion. Two refractory metal electrodes serve as the ion optics and the hollow cathode assemblies are derived from the plasma contactor and NSTAR programs. Tests were conducted in Vacuum Facility 16 (VF16), which is a 2.7 m diameter by 8.5 m long facility with a base pressure of 1.5×10^{-5} Pa (1.1×10^{-7} torr). The thruster was operated manually with commercial power supplies and mass flow controllers, and thruster telemetry was recorded at 0.5 Hz using a data acquisition and control system. Full details of the test set-up are detailed in Reference 24. The Dev-C thruster was mounted within VF-16 using a rigid three-point mounting system, as shown in Figure 26(a).

The thrust vector probe system consisted of an 18×18 array of graphite rods, with a diameter of 0.19 cm and a length of 15.2 cm. Each rod had an identical surface finish and small radial tolerance (1 mil = 0.0254 mm) due to the center-less grinding technique used to machine the rods. The probes were mounted within a stainless steel frame 719.5 cm downstream of the exit plane of the thruster, and biased -30 V below Earth ground to repel electrons. The probe frame was lined with graphite-based material and shadow shields were used to electrically isolate the probes from the frame. A Type-K thermocouple was placed on the backside of the probe frame to measure the temperature during thruster operation. The current collected by each rod was measured across a shunt bank consisting of 36 precision 1 k Ω resistors. The system was calibrated by passing known currents through the cabling and shunt bank. A laser alignment tool was used to align the thruster with the probe array. The probes were mounted within VF-16 as shown in Figure 26(b).

Test Results and Discussion

Tests were performed using the standard NEXT throttle table, which consists of discrete operating points that are defined by a unique combination of the beam current and the beam power supply voltage (Ref. 25). The test matrix was bound by operating the thruster at the lowest discharge power (TL01), the highest discharge power (TL37), an intermediate input power level (TL28), and the highest total input power (TL40). Collected probe currents are shown in Figure 27 for steady-state operation at TL28. The data are well described by Gaussian curve fits, and the beam centroid uncertainties were on the order of 3 to 6 mm, which corresponds to an uncertainty of 0.1° in the calculated thrust vector angle.

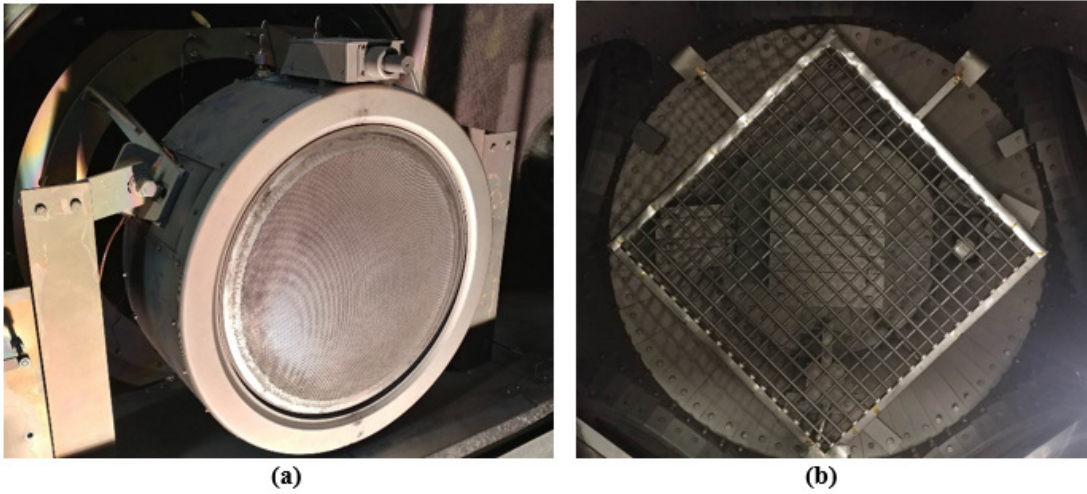


Figure 26.—(a) Dev-C thruster mounted in VF16. (b) Far-field thrust vector probe array.

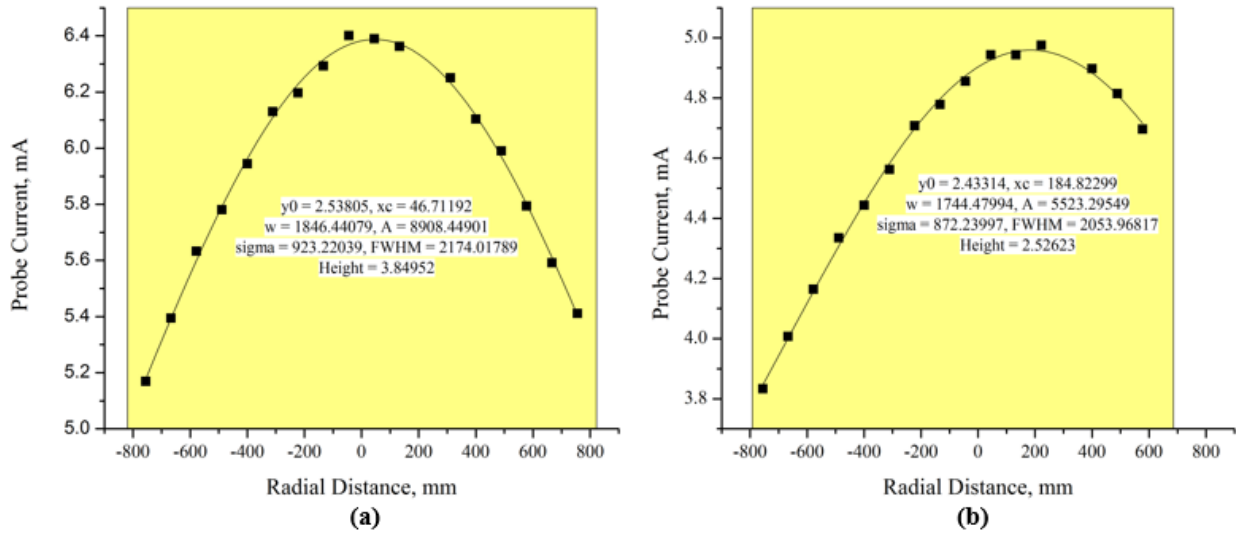


Figure 27.—Measured probe currents for both the horizontal and vertical array of probes during steady state operation at TL28.

Figure 28(a) shows the thrust vector behavior during a start-up at TL28 (similar behavior was observed at higher power levels). In the plot, $t = 0$ corresponds to the application of high voltage. Within seconds of applying high voltage, an offset angle of 1° was observed. This offset may be due to plasma distribution asymmetries in the discharge chamber and/or slight mechanical misalignment of the optics due to manufacturing tolerances. The thrust vector angle increases to a maximum of 1.7° after 25 min of thruster operation and slowly decreases to 1.5° as the thruster reaches thermal equilibrium. The Dev-C thruster was instrumented with thermocouples during prior developmental tests and it is informative to investigate the measured thruster temperatures when the engine was operated in an identical manner. Figure 28(b) shows the thermocouple data, which includes temperature data from the discharge chamber (Tdc1), the front mask (Tms1), and both the screen and accelerator grids (Tg1 and Tg2). There is excellent qualitative agreement between the thrust vector angle and the difference in the grid temperature (Tg1-Tg2), suggesting that differential grid movement dominates thrust vector offsets during the first few hours of operation. This time-resolved behavior is consistent with data obtained with other ion engines.

The data from the tests can be used to bound the thrust vector offsets. The offsets during start-ups and throttling were less than 2.0° and the steady-state deviation was on the order of 0.2° to 0.3° . Similar magnitudes were obtained with an engineering model engine (not reported herein). The data were found to be highly repeatable, with variations within the measurement error (0.12°). Preliminary data suggests that the $\pm 5^\circ$ gimbal range used with the NSTAR engine would be adequate for the NEXT system, although further analysis may be necessary to quantify thrust vector drift over longer periods of thruster operation.

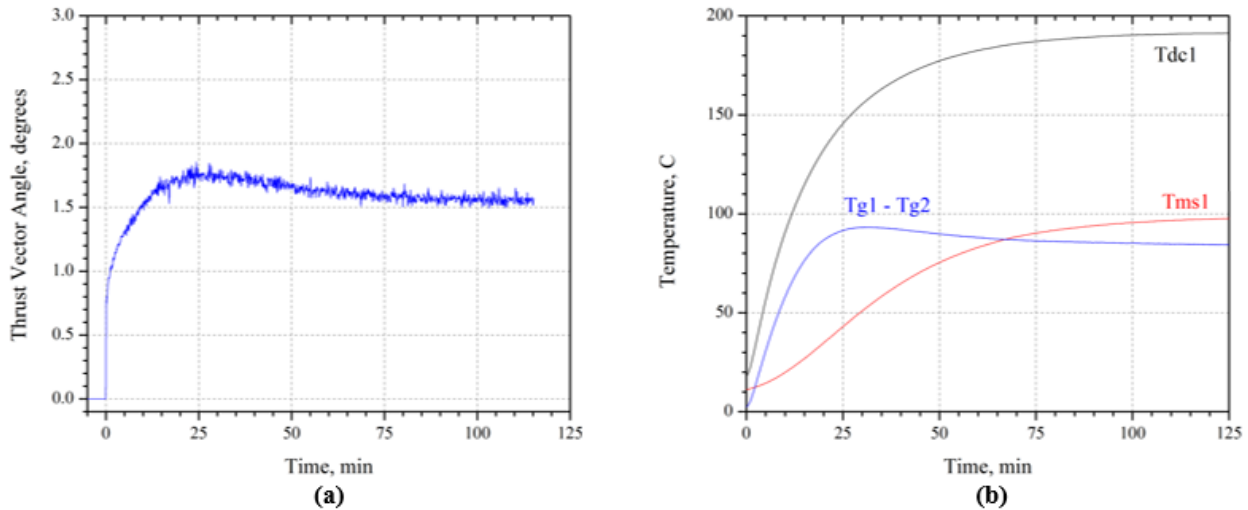


Figure 28.—(a) Thrust vector behavior during a start-up at TL28. (b) Corresponding thermocouple data as the thruster reaches thermal equilibrium.

References

1. Smith, B.K., Nazario, M.L., and Cunningham, C.C., “Solar Electric Propulsion Vehicle Demonstration to Support Future Space Exploration Missions,” *Space Propulsion 2012*, Bordeaux, France, 2012.
2. Herman, D.A., Tofil, T., Santiago, W., Kamhawi, H., Polk, J.E., Snyder, J.S., Hofer, R.R., Picha, F., Jackson, J., and Allen, M., “Overview of the Development and Mission Application of the Advanced Electric Propulsion System (AEPS),” *35th International Electric Propulsion Conference*, IEPC Paper 2017-284, Electric Rocket Propulsion Society, Fairview Park, OH, 2017.
3. Polk, J.E., Anderson, J.R., and Brophy, J.R., “Behavior of the Thrust Vector in the NSTAR Ion Thruster,” *34th AIAA/ASME/SAE/ASEE Joint Propulsion Conference and Exhibit*, AIAA Paper 1998-3940, Cleveland, OH, 1998.
4. Polk, J.E., Anderson, J.R., and Brophy, J.R., “Behavior of the Thrust Vector in the NSTAR Ion Thruster,” *34th AIAA/ASME/SAE/ASEE Joint Propulsion Conference and Exhibit*, AIAA Paper 1998-3940, Cleveland, OH, 1998.
5. Snyder, J.S., Goebel, D.M., Hofer, R.R., Polk, J.E., Wallace, N.C., and Simpson, H., “Performance Evaluation of the T6 Ion Engine,” *Journal of Propulsion and Power*, Vol. 28, No. 2, 2012, pp. 371–379.
6. Pollard, J.E., “Beam-Centroid Tracking Instrument for Ion Thrusters,” The Aerospace Corporation, Aerospace Report No. TR-94(4507)-1, 20 March 1995.
7. Pollard, J.E. and Welle, R.P., “Thrust Vector Measurements with the T5 Ion Engine,” *31st AIAA/ASME/SAE/ASEE Joint Propulsion Conference and Exhibit*, AIAA Paper 1995-2829, San Diego, CA, 1995.
8. Pollard, J.E. and Beiting, E.J., “Ion Energy, Ion Velocity, and Thrust Vector Measurements for the SPT-140 Hall Thruster,” *Proc. of the 3rd International Conference on Spacecraft Propulsion*, European Space Agency, Cannes, France, 2000, pp. 789–796.
9. Pollard, J.E., “Profiling the Beam of the T5 Ion Engine,” *25th International Electric Propulsion Conference*, IEPC Paper 97-019, Electric Rocket Propulsion Society, Fairview Park, OH, 1997.
10. Muravlev, V.A., Khabibullin, E.R., and Shutov, V.N., “The Device for Electric Propulsion Lateral Thrust Vector Components Measurement,” *32nd International Electric Propulsion Conference*, IEPC Paper 2011-026, Electric Rocket Propulsion Society, Fairview Park, OH, 2011.
11. Gnizdor, R., Komarov, A., Pridannikov, S., and Savchenko, K., “Investigation of the thruster vector angle stability of the stationary plasma thrusters,” *35th International Electric Propulsion Conference*, IEPC Paper 2017-41, Electric Rocket Propulsion Society, Fairview Park, OH, 2017.
12. Weis, S., Lazurenko, A., Genovese, A., Heidemann, R., Holtmann, P., Stalzer, H., Püttmann, N., Wolf, T., and Wollenhaupt, B., “Overview, Qualification and Delivery Status of the HEMP-Thruster based Ion Propulsion System for SmallGEO,” *35th International Electric Propulsion Conference*, IEPC Paper 2017-197, Electric Rocket Propulsion Society, Fairview Park, OH, 2017.
13. Van Reijen, B., Weis, S., Lazurenko, A., Haderspeck, J., Genovese, A., Holtmann, P., Ruf, K., and Püttmann, N., “High Precision Thrust Vector Determination through Full Hemispherical RPA Measurements assisted by Angular Mapping of Ion Energy Charge State Distribution,” *33rd International Electric Propulsion Conference*, IEPC Paper 2013-284, Electric Rocket Propulsion Society, Fairview Park, OH, 2013.
14. Pagano, D., Coduti, G., Scaranzin, S., Meniconi, G., Scortecci, F., and Kutufa, N., “Performance of Plume Characterization of the SPT100-B Thruster,” *34th International Electric Propulsion Conference*, IEPC Paper 2015-10, Electric Rocket Propulsion Society, Fairview Park, OH, 2015.
15. Lazurenko, A., van Reijen, B., Koch, N., Weis, S., Genovese, A., Haderspeck, J., Schirra, M., Scaranzin, S., Bonelli, E., and Scortecci, F., “Overview on Testing Infrastructures and Diagnostic Tools for HEMPT based Ion Propulsion Systems,” *32nd International Electric Propulsion Conference*, IEPC Paper 2011-146, Electric Rocket Propulsion Society, Fairview Park, OH, 2011.

16. Moneti, F., Bonelli, E., Pulcinelli F., Scortecchi F., Lazurenko, A., and Genovese, A., “Performance of Aerospazio Lifetest Facilities and Diagnostic Tools for the HEMPT Qualification Programme,” *35th International Electric Propulsion Conference*, IEPC Paper 2017-483, Electric Rocket Propulsion Society, Fairview Park, OH, 2017.
17. Scortecchi, F., Bonelli E., Michelozzi B., Saito, F., Scaranzin, S., and Turco, A., “Performance of a Large Vacuum Facility for Spacecraft Propulsion Testing,” *Proc. of the 4th Int. Spacecraft Propulsion Conference*, European Space Agency, Cagliari, Sardinia, Italy, 2004.
18. Huang, W., Kamhawi, H., Haag, T.W., Ortega, A.L., and Mikellides, I.G., “Facility Effect Characterization Test of NASA’s HERMeS Hall Thruster,” *52nd AIAA/SAE/ASEE Joint Propulsion Conference*, AIAA Paper 2016-4828, Salt Lake City, UT, 2016.
19. Sohl, G. and Forsnight, V.V., “Thrust Vectoring of Ion Engines,” *J. Spacecraft*, Vol. 6, No. 2, 1969, pp. 143–147.
20. Homa, J.M and Wilbur, P.J, “Ion Beamlet Vectoring by Grid Translation,” *AIAA/JSASS/DGLR 16th International Electric Propulsion Conference*, AIAA Paper 1982-1895, New Orleans, LA, 1982.
21. Haag, T., “Translation Optics for 30 cm Ion Engine Thrust Vector Control,” *27th International Electric Propulsion Conference*, IEPC Paper 01-116, Pasadena, CA, 2001.
22. Hoskins, W.A., Wilson, F.C., Polaha, J., Talerico, L., Patterson, M.J., Soulas, G.C., and Sovey, J., “Development of a Prototype Model Ion Thruster for the NEXT System,” *40th AIAA/ASME/SAE/ASEE Joint Propulsion Conference and Exhibit*, AIAA Paper 2004-4111, Fort Lauderdale, FL, 2004.
23. Herman, D.A., Soulas, G.C., and Patterson, M.J., “Performance Evaluation of the Prototype-Model NEXT Ion Thruster,” *43rd AIAA/ASME/SAE/ASEE Joint Propulsion Conference & Exhibit*, AIAA Paper 2007-5212, Cincinnati, OH, 2007.
24. Shastry, R., Herman, D.A., Soulas, G.C., and Patterson, M.J., “End of Test Performance and Wear Characterization of NASA’s Evolutionary Xenon Thruster (NEXT) Long Duration Test,” *50th AIAA/ASME/SAE/ASEE Joint Propulsion Conference*, AIAA Paper 2014-3617, Cleveland, OH, 2014.
25. Patterson, M.J., Soulas, G.C., Young, J.A., and Crofton, M.W., “Expanded Throttling Capabilities of the NEXT Thruster,” *49th AIAA/ASME/SAE/ASEE Joint Propulsion Conference*, AIAA Paper 2013-3891, San Jose, CA, 2013.

